Full-Wave Analysis of Coupled Perfectly Conducting Wires in a Multilayered Medium

Niels Faché, Frank Olyslager, *Student Member, IEEE*, and Daniël De Zutter

Abstract—**This paper presents a full-wave analysis of coupled perfectly conducting cylindrical wires in a multilayered dielectric medium. The analysis is based on a Fourier series expansion of the unknown surface currents on each wire and on an integral equation for the longitudinal field on the wires. The calculations are not restricted to the propagation constants of the different modes, but explicit results are presented for the impedances associated with each wire and each eigenmode and this as a function of frequency. Propagation constants, longitudinal currents on the wires and impedances lead to a complete circuit equivalent for the structures being considered.**

I. Introduction

MICROSTRIPS and striplines play an important role in high-speed digital as well as high-frequency analog applications. Much theoretical effort has been expended in modeling these structures both in the quasi-TEM limit [1] and in the full-wave regime [2]–[4], [11]. An alternative to printed circuit lines is the use of discrete wire technology. Two important applications of this technique are the multiwire and microwire boards which allow the controlled impedance transport of very high speed signals in very dense circuits [5], [6].

This paper presents a full-wave analysis of coupled wire transmission lines in a multilayered dielectric medium. We first determine the propagation constants of the fundamental eigenmodes associated with the coupled wires. In a second step, special emphasis is placed on the determination of the impedances of these modes and their frequency dependence. To this end, it is necessary to determine the total complex power propagated by each mode. To the best of the authors' knowledge, this is the first time that frequency-dependent impedance results are presented for wire structures. Combining the knowledge of propagation constants and impedances as a function of frequency and of the values of the total longitudinal currents on each wire, it becomes possible to derive a complete coupled transmission line equivalent circuit for the configurations under study. The results presented in this paper constitute a substantial extension of the restricted analysis presented in [7]. For quasi-TEM results on a single wire and on two coupled wires, the reader is referred to [8] and [9].

Manuscript received January 17, 1990; revised November 29, 1990. This work was supported by the Instituut tot Aanmoediging van het Onderzoek in de Lanbouw en de Nijverheid through a grant to N. Faché. D. De Zutter and F. Olyslager are Research Associates of the National Fund for Scientific Research of Belgium.

The authors are with the Laboratory of Electromagnetism and Acoustics, University of Ghent, Sint-Pietersnieuwstraat 41, 9000 Ghent, Belgium.

IEEE Log Number 9042501.

II. Geometry of the Problem

The geometry of the cross section of the multilayered interconnection structure under consideration is shown in Fig. 1. It consists of L homogeneous layers with arbitrary thickness d_i, permittivity ϵ_i, and permeability μ_i $(i = 1, \cdots, L)$. We distinguish structures of the covered type (Fig. 1(a)), of the semiopen type (Fig. 1(b)) and of the open type (Fig. 1(c)). The metallic planes are perfectly conducting. This is also the case for the W interconnection wires. Each wire is fully embedded in a single layer. The coordinate system is indicated on the figure. In what follows, we will often refer to the interaction between two wires. Two such wires are shown in Fig. 2. One wire will be called the source wire. This wire and the layer in which it is located are indicated by the letters s and t respectively. The second will be called the observation wire o located in layer p.

III. General Outline of the Solution

The purpose of this paper is to calculate the W lowest eigenmodes associated with the interconnection structure consisting of W wires embedded in a multilayered medium. For one such eigenmode, all field components depend upon x through the common phase factor $\exp(-j\beta x)$, where β represents the propagation constant. The field can be written as

$$\begin{aligned} \boldsymbol{e}(x,y,z) &= \boldsymbol{E}(y,z)\exp(-j\beta x) \\ \boldsymbol{h}(x,y,z) &= \boldsymbol{H}(y,z)\exp(-j\beta x). \end{aligned} \tag{1}$$

The common time dependence $\exp(j\omega t)$ and the common phase factor $\exp(-j\beta x)$ are suppressed throughout this paper. As for the single wire [7], the determination of an eigenmode starts from the surface currents on each wire. In what follows, we will regard the problem as the superposition of the action of W source wires. The surface currents on each source wire are $J_{x,s}(r_s, \phi_s)$. As shown in Fig. 2, we refer these surface currents to a local coordinate system (r_s, ϕ_s) associated with each wire. For each source wire we first determine the fields associated with the as yet unknown surface currents on that wire. These fields are found as the sum of two contributions. A first contribution, the incoming fields $\boldsymbol{E}_t^{\text{in}}(y, z; \boldsymbol{J}_s)$ and $\boldsymbol{H}_t^{\text{in}}(y, z; \boldsymbol{J}_s)$, are those fields that we find when the source wire s under consideration is placed in a homogeneous space with the same electric and magnetic properties as the layer t in which the source wire is located.

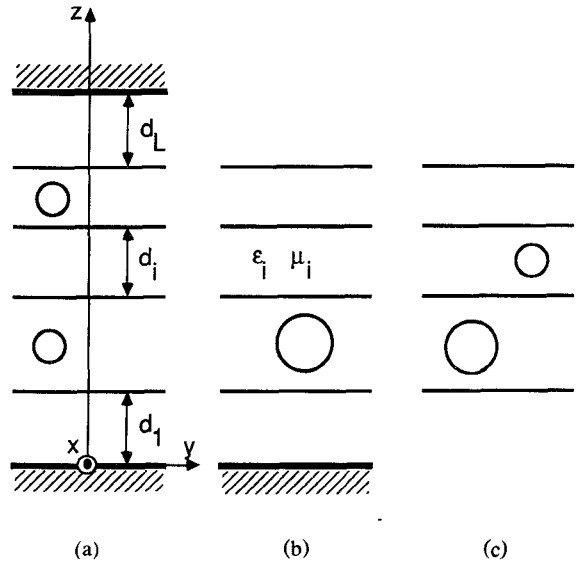

Fig. 1. Cross section of the coupled wire transmission lines in a multilayered medium: (a) closed structure; (b) semi-open structure; (c) open structure.

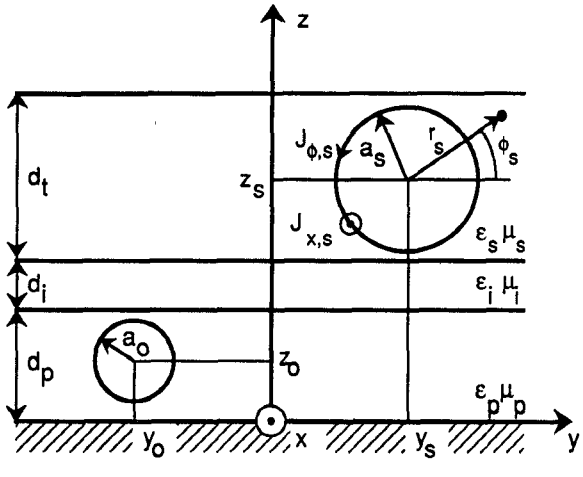

Fig. 2. Excitation and observation wire and associated coordinates.

In this operation the original unknown surface currents $J_{x,s}$ and $J_{\phi,s}$ are left unaltered. In order to emphasize the fact that these incoming fields are determined in the layer t, we use the subscript t with these incoming fields. The second contribution is found by taking into account the layered nature of the original medium. This is done by considering the scattering of the incoming fields by the layered medium. This results in the scattered fields $\boldsymbol{E}_i^{sc}(y, z; \boldsymbol{J}_s)$ and $\boldsymbol{H}_i^{sc}(y,z; \boldsymbol{J}_s)$. The subscript i now indicates the fact that these scattered fields exist in each layer i of the medium ($i = 1, \cdots, L$). In a last step, the superposition of the fields from all the wires yields the total electric and magnetic fields everywhere. In each layer i these total fields are given by

$$\boldsymbol{E}_i^{to}(y,z) = \sum_{s=1}^{s=W} \left(\delta_{t,i}\boldsymbol{E}_t^{in}(y,z;\boldsymbol{J}_s) + \boldsymbol{E}_i^{sc}(y,z;\boldsymbol{J}_s)\right)$$

$$\boldsymbol{H}_i^{to}(y,z) = \sum_{s=1}^{s=W} \left(\delta_{t,i}\boldsymbol{H}_t^{in}(y,z;\boldsymbol{J}_s) + \boldsymbol{H}_i^{sc}(y,z;\boldsymbol{J}_s)\right). \quad (2)$$

The summation in (2) extends over all wires. The symbol $\delta_{t,i}$ is the well-known Kronecker delta. In order to finally determine the eigenmodes and associated eigenvalues we impose the boundary conditions on each wire surface, using Galerkin's method. This leads to the relevant integral equation for the eigenmodes of the configuration under consideration. In the next section some details are given on each step in the calculation.

IV. Incoming Fields in the Space Domain

Using Green's theorem and the Green's function for a homogeneous space with the same properties as the layer t in which one particular source wire s is located, the longitudinal x components of the incoming electric and magnetic field can be written as [7], [10]

$$E_{x,t}^{in}(\boldsymbol{r}) = \int_0^{2\pi} \left[G_t \frac{\partial E_{x,t}^{to}(a_s,\phi_s)}{\partial r_s} \right] a_s \, d\phi_s \quad (3)$$

and

$$H_{x,t}^{in}(\boldsymbol{r}) = -\int_0^{2\pi} \left[H_{x,t}^{to}(a_s,\phi_s) \frac{\partial G_t}{\partial r_s} \right] a_s \, d\phi_s \quad (4)$$

with $\boldsymbol{r} = y\boldsymbol{u}_y + z\boldsymbol{u}_z$ and a_s the radius of the source wire. The superscript "to" describes a total field component. The integration in (3) and (4) extends over the circumference of wire s, and G_t is given by

$$G_t = \frac{j}{4} H_0^{(2)}(\gamma_t |\boldsymbol{a}_s - \boldsymbol{r}|) \quad (5)$$

where $\boldsymbol{a}_s$ is a running integration point on the wire surface and

$$\gamma_t^2 = \omega^2 \epsilon_t \mu_t - \beta^2. \quad (6)$$

The quantity γ_t is defined as the root of γ_t^2 with a nonnegative real part and a nonpositive imaginary part. $H_0^{(2)}$ represents the Hankel function of the second kind and of order zero. As in [7], it turns out that all field components of the incoming as well as of the scattered fields can be expressed in terms of the x components of these fields. From (3) and (4) it is clear that $\partial E_{x,t}^{to}/\partial r_s$ and $H_{x,t}^{to}$ on the wire surface are the actual basic unknowns of our problem. These quantities are of course directly related to the surface currents $J_{x,s}$ and $J_{\phi,s}$ and it is only a matter of convenience which set of unknowns is used. We expand the unknown functions in an angular Fourier series:

$$\frac{\partial E_{x,t}^{to}(\boldsymbol{a}_s)}{\partial r_s} = \sum_{n=-\infty}^{n=+\infty} A_{n,s} \exp(jn\phi_s) \quad (7)$$

and

$$H_{x,t}^{to}(\boldsymbol{a}_s) = \sum_{n=-\infty}^{n=+\infty} B_{n,s} \exp(jn\phi_s). \quad (8)$$

Inserting (7) and (8) into (3) and (4) leads to [7]

$$E_{x,t}^{in}(\boldsymbol{r}) = \sum_{n=-\infty}^{n=+\infty} C_{n,s} H_n^{(2)}(\gamma_t r_s) \exp(jn\phi_s)$$

$$H_{x,t}^{in}(\boldsymbol{r}) = \sum_{n=-\infty}^{n=+\infty} D_{n,s} H_n^{(2)}(\gamma_t r_s) \exp(jn\phi_s) \quad (9)$$

where $H_n^{(2)}$ represents the Hankel function of the second

kind and of order n, and r is now given in reference to its coordinates r_s and ϕ_s in the local coordinate system of wire s. In addition,

$$C_{n,s} = \frac{ja_s\pi}{2} J_n(\gamma_t a_s) A_{n,s}$$

$$D_{n,s} = -\frac{ja_s\pi}{2} \gamma_t J_n'(\gamma_t a_s) B_{n,s} \tag{10}$$

where J_n represents the Bessel function of order n.

V. Incoming Fields in the Spectral Domain

In the above section we have calculated the incoming fields originating from one particular source wire s. To determine the total fields at the surface of the wires we have to calculate the contribution of each source wire to the total field at the surface of any other wire. In what follows, such a wire is indicated as observation wire o. If the observation wire is located in the same layer as the source wire, the incoming fields contribute directly to the total fields at the observation wire. This contribution will be discussed in Section VI. If the observation wire is located in a different layer, the scattering of the incoming field must be taken into account. These scattered fields also contribute to the total fields at the source wire itself. Scattered fields will be discussed in Section VII. In both cases we need the incoming fields in the spectral domain. To this end we introduce the spatial Fourier transformation of all fields with respect to the lateral y direction. For the incoming fields (9) this spatial Fourier transformation can be performed analytically. We refer the reader to [7, appendix II] for details on the calculations:

$$E_{x,t}^{\text{in}}(k_y, z) = \frac{\exp\left[\alpha\Gamma_t(z - z_s) + jk_y y_s\right]}{\Gamma_t} \cdot \sum_{n=-\infty}^{n=+\infty} (j/\pi)(\alpha)^n C_{n,s} \left(\frac{\Gamma_t - \alpha k_y}{\Gamma_t + \alpha k_y}\right)^{n/2}$$

$$H_{x,t}^{\text{in}}(k_y, z) = \frac{\exp\left[\alpha\Gamma_t(z - z_s) + jk_y y_s\right]}{\Gamma_t} \cdot \sum_{n=-\infty}^{n=+\infty} (j/\pi)(\alpha)^n D_{n,s} \left(\frac{\Gamma_t - \alpha k_y}{\Gamma_t + \alpha k_y}\right)^{n/2} \tag{11}$$

where y_s and z_s are indicated in Fig. 2. Below the source wire α takes the value 1 and above the source wire the value -1. In (11), k_y is the spatial Fourier variable and Γ_t is defined as the root with nonnegative real and nonnegative imaginary parts of $(k_y^2 - \gamma_t^2)$.

VI. Incoming Fields at an Observation Wire Located in the Source Layer

The actual situation is depicted in Fig. 3. The figure shows two wires. The rightmost wire is the source wire s. The leftmost wire is an observation wire o located in the same layer. Instead of using the original (r_s, ϕ_s) coordinate system on each wire, as shown in Fig. 3 we introduce new (y', z') axes with their origin at the center of the source wire. The z' axis is directed from the center of the source wire to the center of the observation wire. The new polar angles are now

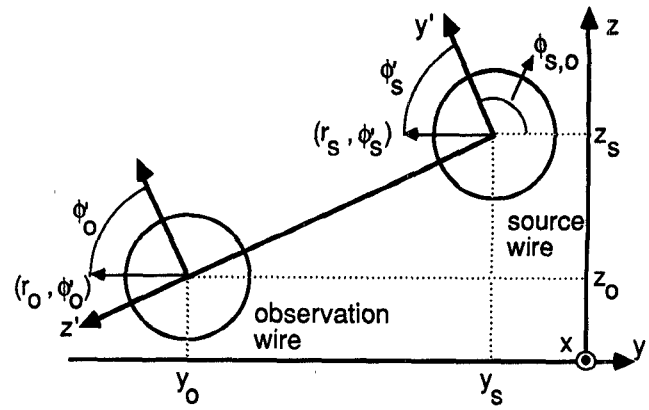

Fig. 3. Coordinate system used in the calculation of the incoming field at an observation wire located in the source layer.

measured with respect to the y' axis:

$$\phi'_s = \phi_s - \Phi_{s,o} \quad \text{and} \quad \phi'_o = \phi_o - \Phi_{s,o}. \tag{12}$$

The subscript s still indicates the source wire, while the subscript o will be used to indicate an observation wire. The angle $\Phi_{s,o}$ is defined in Fig. 3. The x component of the incoming electric field (9) can be rewritten as

$$E_{x,t}^{\text{in}}(r) = \sum_{n=-\infty}^{n=+\infty} C_{n,s} \exp(jn\Phi_{s,o}) H_n^{(2)}(\gamma_t r_s) \exp(jn\phi'_s). \tag{13}$$

As in the above section on the spectral incoming fields, we calculate the spatial Fourier transformation of (13) but now with respect to the y' coordinate. This leads to

$$E_{x,t}^{\text{in}}(k'_y, z') = \frac{\exp\left[-\Gamma_t(z' - d_{s,o})\right]}{\Gamma_t} \sum_{n=-\infty}^{n=+\infty} (j/\pi) C_{n,s} \cdot \exp(jn\Phi_{s,o}) \left(\frac{\Gamma_t + k'_y}{\Gamma_t - k'_y}\right)^{n/2}. \tag{14}$$

We have used the spectral variable k'_y to emphasize the fact that the transformation applies to the y' coordinate. The distance $d_{s,o}$ between the centers of the source and the observation wire is given by

$$d_{s,o} = \left[(y_s - y_o)^2 + (z_s - z_o)^2\right]^{1/2}. \tag{15}$$

Expression (14) allows us to explicitly determine the spatial fields at the observation wire. Analogous reasoning can be applied to the magnetic field. If we write the longitudinal fields on the observation wire caused by the incoming fields of the source wire in the following way:

$$E_{x,t}^{\text{in}}(r_o) = \sum_{n=-\infty}^{n=+\infty} E_{n,s}^o \exp(jn\phi_o)$$

$$H_{x,t}^{\text{in}}(r_o) = \sum_{n=-\infty}^{n=+\infty} F_{n,s}^o \exp(jn\phi_o) \tag{16}$$

the Fourier coefficients are found to be

$$E^o_{n,s} = \exp(-jn\Phi_{s,o} - \Gamma_t d_{s,o}) J_n(\gamma_t a_o) \cdot \int_{-\infty}^{+\infty} \left\{ \sum_{m=-\infty}^{m=+\infty} [(jC_{m,s})/(\pi\Gamma_t)] \cdot \left(\frac{\Gamma_t - k_y}{\Gamma_t - k_y} \right)^{(m-n)/2} \right\} dk_y \quad (17)$$

and

$$F^o_{n,s} = \exp(-jn\Phi_{s,o} - \Gamma_t d_{s,o}) J_n(\gamma_t a_o) \cdot \int_{-\infty}^{+\infty} \left\{ \sum_{m=-\infty}^{m=+\infty} [(jD_{m,s})/(\pi\Gamma_t)] \cdot \left(\frac{\Gamma_t - k_y}{\Gamma_t - k_y} \right)^{(m-n)/2} \right\} dk_y. \quad (18)$$

the notation r_o indicates a point on the observation wire and a_o is the radius of that wire. It must be emphasized that $E^o_{n,s}$ depends upon all unknown coefficients $A_{m,s}$ (eq. (7)) and $F^o_{n,s}$ upon all $B_{m,s}$ values (eq. (8)), where $m = 0, \pm 1, \pm 2, \cdots$.

VII. Scattered Fields

In order to find the total fields at the surface of each wire, we finally have to determine the contribution from the scattered fields. Here two different situations have to be considered. If we again start from one particular source wire, we first have to determine the scattered fields at the source wire itself. In this case source and observation wire coincide. A second part of the calculations consists in determining the scattered fields at an observation wire not coinciding with the source wire. This observation wire can be located either inside the same layer as the source wire or in a different layer. We will not go into detail at this point. Starting from the spectral-domain expressions (11), the scattering problem can be solved in the spectral domain by using a TE–TM mode decomposition. We refer the reader to [7] and [11] for additional details on the method. Indicating the layer in which an observation wire is located as layer p, the longitudinal scattered fields take the following general form inside that layer:

$$E^{sc}_{x,p}(k_y, z) = T(k_y)\exp[-\Gamma_p(z - z_o)] + U(k_y)\exp[\Gamma_p(z - z_o)]$$
$$H^{sc}_{x,p}(k_y, z) = V(k_y)\exp[-\Gamma_p(z - z_o)] + W(k_y)\exp[\Gamma_p(z - z_o)] \quad (19)$$

where z_o is indicated in Fig. 2. Detailed calculations for T, U, V, and W are given in [12]. In what follows we will simply assume that they are known functions of the spectral variable k_y and of z. The scattered fields at the surface of the observation wire can be written as the following Fourier series:

$$E^{sc}_{x,p}(r_o) = \sum_{n=-\infty}^{n=+\infty} G^o_{n,s}\exp(jn\phi_o)$$
$$H^{sc}_{x,p}(r_o) = \sum_{n=-\infty}^{n=+\infty} H^o_{n,s}\exp(jn\phi_o). \quad (20)$$

Starting from (19), the values of the Fourier coefficients turn out to be

$$G^o_{n,s} = J_n(\gamma_p a_o)\int_{-\infty}^{+\infty} \exp(-jk_y y_o) \cdot \left[T(k_y)(-1)^n \left(\frac{\Gamma_p - k_y}{\Gamma_p + k_y} \right)^{n/2} + U(k_y) \left(\frac{\Gamma_p + k_y}{\Gamma_p - k_y} \right)^{n/2} \right] dk_y \quad (21)$$

and

$$H^o_{n,s} = J_n(\gamma_p a_o)\int_{-\infty}^{+\infty} \exp(-jk_y y_o) \cdot \left[V(k_y)(-1)^n \left(\frac{\Gamma_p - k_y}{\Gamma_p + k_y} \right)^{n/2} + W(k_y) \left(\frac{\Gamma_p + k_y}{\Gamma_p - k_y} \right)^{n/2} \right] dk_y. \quad (22)$$

We again refer to Fig. 2 for the value of y_o. We draw attention to the fact that $G^o_{n,s}$ and $H^o_{n,s}$ depend upon both the unknown $A_{m,s}$ (eq. (7)) and $B_{m,s}$ (eq. (8)) coefficients.

VIII. Solution of the Eigenproblem

According to (2) the total field at each observation wire is the sum of contributions from the incoming field from that wire, from the incoming fields from source wires located in the same layer as the observation wire, and from the scattered fields caused by all the wires. Collecting results (9), (16), and (20) leads to

$$E^{to}_{x,p}(r_o) = \sum_{n=-\infty}^{n=+\infty} \left(\sum_{s=1}^{s=W} \left(\delta_{o,s} C_{n,s} H^{(2)}_n(\gamma_t a_s) + \delta_{p,t} E^o_{n,s} + G^o_{n,s} \right) \right) \exp(jn\phi_o) \quad (23)$$

and

$$H^{to}_{x,p}(r_o) = \sum_{n=-\infty}^{n=+\infty} \left(\sum_{s=1}^{s=W} \left(\delta_{o,s} D_{n,s} H^{(2)}_n(\gamma_t a_s) + \delta_{p,t} F^o_{n,s} + H^o_{n,s} \right) \right) \exp(jn\phi_o). \quad (24)$$

The notation r_o and the subscript p express the fact that the fields are calculated on the surface of an observation wire located in layer p. In summing up over all wires, contribution (9) has to be taken into account only once when source and observation wire o coincide, and contribution (16) has to be taken into account each time a source wire is located in the same layer as a different observation wire. The total fields (23) and (24) must satisfy the boundary condition on each wire; i.e., $E^{to}_{x,p}(r_o)$ must be zero and $H^{to}_{x,p}(r_o)$ must take the original value (8) we started our calculations from. Applying Galerkin's method, we enforce these boundary conditions for

a limited number of Fourier coefficients per wire. If we limit the sums in (23) and (24) to $|n| \leq N$, we arrive at a set of $W(4N+2)$ equations in an equal number of unknowns $A_{n,s}$ and $B_{n,s}$, where $n = 0, \pm 1, \pm 2, \cdots, \pm N$ and $s = 1, 2, \cdots, W$. We have taken an equal number of coefficients on each wire. The total set of equations has only nonzero solutions for discrete eigenvalues β. After determining the eigenvalues, the eigenvectors can be determined; i.e., the $A_{n,s}$ and $B_{n,s}$ values can be found.

IX. Equivalent Circuit Representation of the Coupled Wires

A. Relevant Parameters of the Circuit Model

The coupled wire structure with W wires can be represented by an equivalent circuit consisting of W coupled transmission lines with W propagating modes. Such a circuit representation has also been proposed for coupled strip or microstrip structures. A consistent circuit representation valid up to very high frequencies was developed in [13] by two of the present authors.

The coupled transmission line model for the W lowest order modes of the structure is given by

$$V_i(x) = \sum_{j=1}^{j=W} \left[(Z_{ij}I_{ij})/(Z_{1j}I_{1j})\right]\left[Q_j \exp(-j\beta_j x) + R_j \exp(j\beta_j x)\right]$$

$$I_i(x) = \sum_{j=1}^{j=W} \left[I_{ij}/(Z_{1j}I_{1j})\right]\left[Q_j \exp(-j\beta_j x) - R_j \exp(j\beta_j x)\right]. \tag{25}$$

Here V_i and I_i, $i = 1, 2, \cdots, W$, represent the voltages and currents on the coupled lines, and Z_{ij} is the impedance associated with wire i due to eigenmode j. The β_j are the eigenvalues of the W lowest modes. The unknown but constant coefficients Q_j and R_j are determined by the loading and driving conditions of the lines. The impedances can be found by solving the following set of equations in the V_{ij}'s [13]:

$$\sum_{i=1}^{i=W} V_{ij} I_{ik}^* = P_{jk}, \qquad j, k = 1, \cdots, W. \tag{26}$$

In (25) and (26) I_{ij} represents the current in wire i due to eigenmode j. Each quantity P_{jk} represents the complex power propagating through the structure in the longitudinal direction associated with the electric field of mode j and the magnetic field of mode k. Solving for the V_{ij}'s leads to $Z_{ij} = V_{ij}/I_{ij}$. The reader is referred to [13] for details.

B. Total Longitudinal Currents

The total longitudinal current I_{ij} on wire i caused by eigenmode j can be found from the integration of the ϕ component of the total magnetic field associated with mode j along the circumference of the wire. Using Maxwell's equations to express the ϕ component of the magnetic field in terms of the longitudinal electric and magnetic field components and their derivatives leads to the following final result:

$$I_{ij} = -2a_i j\omega\epsilon A_{0,i}/\gamma_i^2. \tag{27}$$

Here wire i is located in a layer with dielectric constant ϵ and has radius a_i. $A_{0,i}$ is the zeroth-order Fourier coefficient defined in (7) associated with wire i and eigenmode j.

C. Total Propagated Complex Powers

In this subsection we will give a very brief account of the power calculations. The purpose is the calculation of the power terms P_{jk} defined in subsection A. Starting from the projection of Poynting's vector on the longitudinal x direction, P_{jk} is found to be

$$P_{jk} = (1/2)\int_S \int \left\{\left[\boldsymbol{E}_j^{\text{to}} \times \left(\boldsymbol{H}_k^{\text{to}}\right)^*\right] \cdot \boldsymbol{u}_x\right\} dS \tag{28}$$

where the integration extends over the total cross section S of the structure under consideration. The electric field in (28) is the total electric field of eigenmode j, and the magnetic field is the total magnetic field of eigenmode k, as indicated by the subscripts. These fields are themselves superpositions of the fields arising from the individual wires:

$$\boldsymbol{E}_j^{\text{to}}(\boldsymbol{r}) = \sum_{m=1}^{m=W} \boldsymbol{E}_{j,m}^{\text{to}}(\boldsymbol{r})$$

$$\boldsymbol{H}_k^{\text{to}}(\boldsymbol{r}) = \sum_{n=1}^{n=W} \boldsymbol{H}_{k,n}^{\text{to}}(\boldsymbol{r}). \tag{29}$$

This means that P_{jk} can be rewritten in terms of elementary contributions given by

$$P_{jk}^{mn} = (1/2)\int_S \int \left\{\left[\boldsymbol{E}_{j,m}^{\text{to}} \times \left(\boldsymbol{H}_{k,n}^{\text{to}}\right)^*\right] \cdot \boldsymbol{u}_x\right\} dS \tag{30}$$

where $m, n = 1, 2, \cdots, W$. This equation represents the power associated with the electric field of wire m caused by mode j and the magnetic field of wire n caused by mode j. The power contributions P_{jk}^{mn} themselves can be found as the sum of partial power contributions propagated through each layer of the medium. In order to calculate these different partial power terms, the situation depicted in Fig. 4(a) must be distinguished from that depicted in Fig. 4(b). In the first case we consider two wires m and n in the same or in different layers and a layer l which differs from the layers in which m and n are located. In that case the partial power contribution from layer l to P_{jk}^{mn} can be found in the spectral k_y Fourier domain and emerges as a by-product of the scattered field calculations which were outlined in Section VII. In the second case layer l coincides with either the layer in which m is located or the one in which n is located. The actual situation depicted in Fig. 4(b) is the one where the three layers considered coincide. In this case it is no longer advisable to directly integrate in the spectral domain

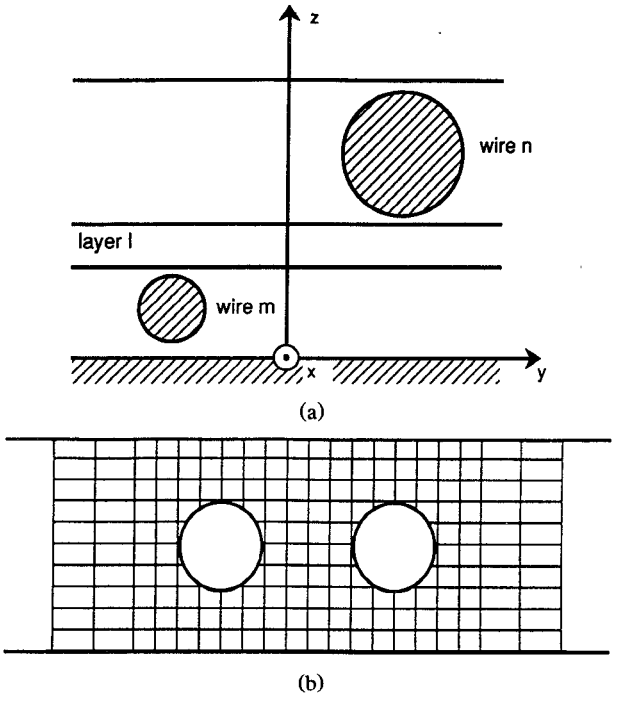

Fig. 4. Wire configurations in the calculation of the propagated power. (a) Two wires m and n located in a different layer. (b) Two wires in the same layer and the associated division of the space into elementary cells.

owing to the complicated z dependence of one or both fields in (30). This is because (11) is not valid aside a wire. The alternative is to integrate in the spatial domain. Fig. 4(b) shows a typical division of the space into elementary cells used for these calculations. We first calculate the values of the electric and magnetic fields in the space domain in the center of gravity of each cell. From this the x component of Poynting's vector in the center is known. Multiplying this value by the cell surface yields the P_{jk}^{mn} value for the cell. In the y direction these cells extend only up to the point where the power contribution of a cell is nonnegligible.

X. Numerical Examples

As a first example we select the single-wire configuration shown in the inset of Fig. 5. The substrate is nonmagnetic with $\epsilon_r = 4$. The ratio of the radius a of the cylinder to the thickness d of the substrate remains fixed at $a/d = 0.25$, while d takes the value 3 mm. Fig. 5 shows the impedance of the normalized propagation constant β/k_0, where $k_0 = \omega/c$, as a function of frequency. Fig. 5(a) gives results for $H/d = 0.5$; i.e., the wire is located in the center of the substrate. Fig. 5(b) gives the corresponding results for $H/d = 1.5$; i.e., the wire is located above the substrate at a height which equals half the substrate thickness. This last configuration can be used to model a bond wire. In both cases the value of the propagation constant already differs quite substantially from its static value before the impedance starts deviating in a considerable way from its quasi-TEM value. From 10 GHz on, however, rapid changes occur for both propagation constants and impedances. This change is especially marked for the configuration of Fig. 5(b). This is due to the fact that dramatic changes take place in the field patterns and the field becomes more and more confined in a

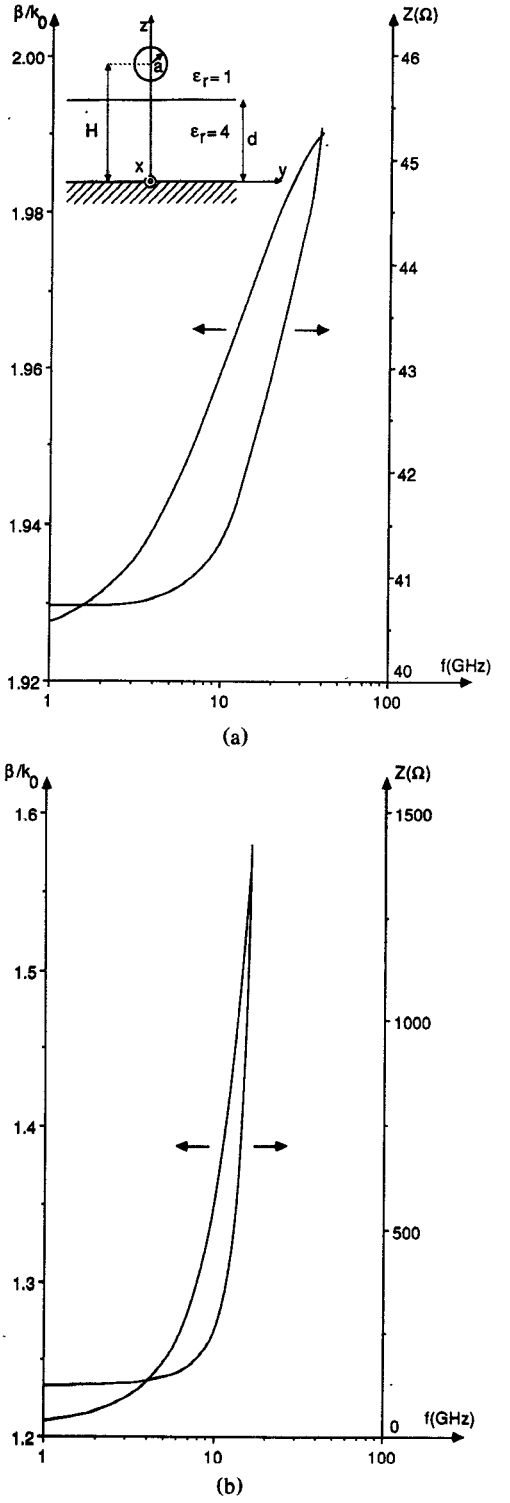

Fig. 5. (a) Circuit parameters of a the single-wire configuration in the inset of the figure as a function of frequency ($a/d = 0.25$, $H/d = 0.5$, $d = 3$ mm). (b) Circuit parameters of a the single-wire configuration in the inset of Fig. 5(a) as a function of frequency ($a/d = 0.25$, $H/d = 1.5$, $d = 3$ mm).

small region under the wire owing to the attraction of the dielectric substrate.

As a second example, we select the two-wire configuration shown in Fig. 6. The relative permittivity of the substrate is $\epsilon_r = 4$ and the frequency is kept constant at 15 GHz. The radius of the wires is $a = 0.75$ mm and the substrate thick-

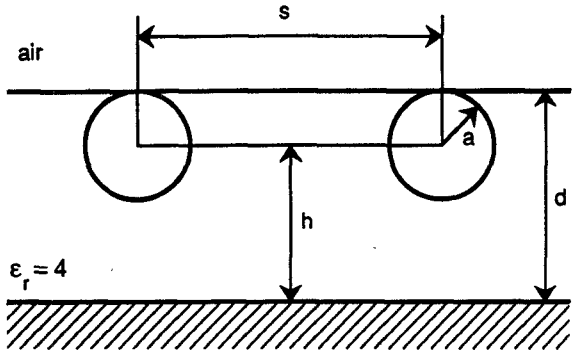

Fig. 6. Two-wire configuration.

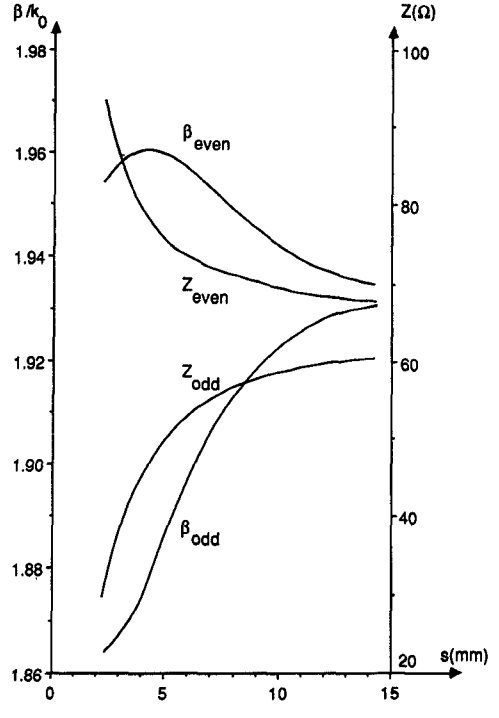

Fig. 7. Circuit parameters for the two-wire configuration of Fig. 6 as a function of the spacing s between the wires ($a/d = 0.25$, $H/d = 0.75$, $d = 3$ mm, $f = 15$ GHz).

ness $d = 3$ mm. The height H takes the value $H = 2.25$ mm. Because of the symmetry of the configuration, the two fundamental modes are the fundamental even and an odd mode of the structure. Fig. 7 shows the (normalized) propagation constants β_{even} and β_{odd} and the impedances Z_{even} and Z_{odd} associated with these modes as a function of the distance between the wires. This distance varies between 2 and 14 mm. Owing to the symmetry $Z_{11} = Z_{21} = Z_{odd}$ and $Z_{12} = Z_{22} = Z_{even}$. For the definitions of Z_{11}, Z_{12}, Z_{21}, and Z_{22} we refer to [13]. For large distances, propagation constants and impedances evolve toward their values for independent, noncoupled wires. For the odd mode the propagation constant increases with increasing distance because an increasing part of the field lines is located between the wires and the ground plane and a decreasing part between the wires. For the even mode the repulsion between the wires decreases as s increases, a larger part of the field is located in the air, and

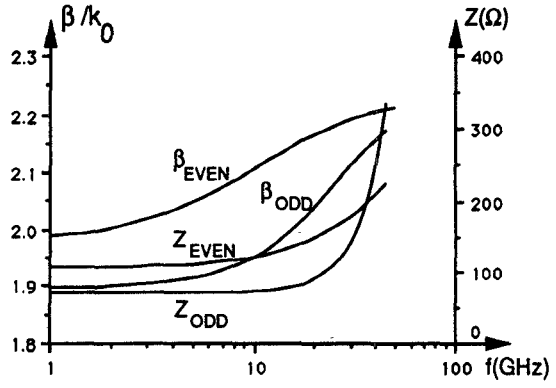

Fig. 8. Circuit parameters for the two-wire configuration of Fig. 6 as a function of frequency ($a = 0.3$ mm, $d = 3$ mm, $s = 3$ mm, $\epsilon_r = 5$).

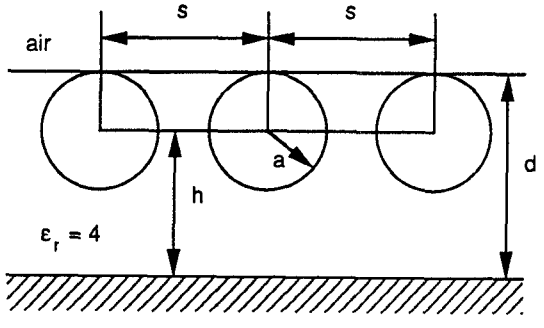

Fig. 9. Three-wire configuration.

β_{even} decreases. However, for wires which are very close to each other ($s < 3.5$ mm), the repulsion becomes very high and field lines start to get pushed into the air again. The final result is that the β_{even} curve exhibits a maximum.

As a third example we again select the configuration of Fig. 6 but with different parameters. The relative permittivity of the substrate now is $\epsilon_r = 5$. The radius of the wires is $a = 0.3$ mm, the substrate thickness is $d = 3$ mm, the spacing between the wires is $s = 3$ mm, and the distance between the ground plane and the wires equals $h = 2.7$ mm. This situation corresponds to one of the situations modeled in the quasi-TEM limit in [9]. In this paper a charge simulation method is used to obtain backward crosstalk data for coupled wires. Fig. 8 shows the values for the propagation constants and impedances as a function of frequency. In the low-frequency limit $\omega \to 0$, we compared our value for the backward crosstalk constant K_b, i.e., $K_b = 0.119$ with the one found in [9], which is about 0.092. K_b is defined as

$$K_b = \left[(Z_{even})^{1/2} - (Z_{odd})^{1/2}\right] \Big/ \left[(Z_{even})^{1/2} + (Z_{odd})^{1/2}\right]. \tag{31}$$

We believe that the difference is due to the better numerical accuracy of the method presented in this paper.

As a last example, we select the configuration of Fig. 9. The relative permittivity of the substrate is again $\epsilon_r = 4$ and the substrate thickness is $d = 3$ mm. The three identical wires have a radius $a = 0.75$ mm, are located at a height $H = 2.25$ mm in the substrate, and have a separation of $s = 2$ mm. Fig. 10 shows the frequency dependence of the

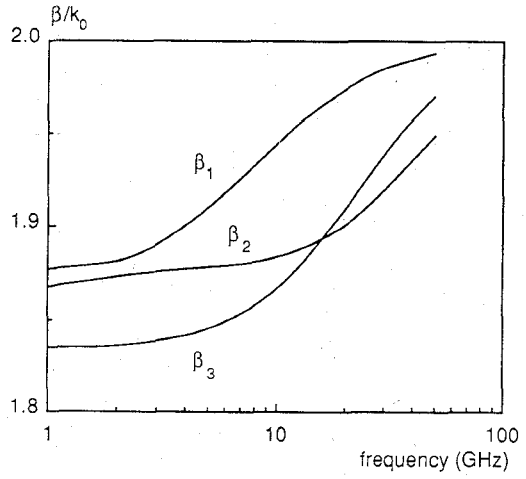

Fig. 10. Propagation constants for the three-wire configuration of Fig. 9 as a function of frequency ($a = 0.75$ mm, $d = 3$ mm, $s = 2$ mm, $\epsilon_r = 4$).

normalized propagation constants β_1, β_2, and β_3 of the so-called first even, second even, and first odd modes. The impedance matrix, as defined in [13], at 1 GHz is given by

$$[Z_{ij}] = \begin{vmatrix} 26.10 & 9.839 & 26.10 \\ 162.4 & 61.235 & 162.4 \\ 38.00 & 3.3\cdot 10^6 & 38.00 \end{vmatrix} \Omega. \qquad (32)$$

XI. Conclusion

In this paper we extended the full-wave analysis for a single wire in a double-layered conductor-backed medium to include not only the propagation constant as a function of frequency but also the impedance as a function of frequency. The analysis was also extended to cover coupled wires and is in fact suited for a multiwire configuration although numerical results were restricted to two wires. The method is also capable of handling a multilayered medium. As the definition of the impedances is based on the power–current formulation, it was necessary to determine the powers and cross-powers propagated by the relevant modes in order to obtain the impedances as a function of frequency. A knowledge of propagation constants, total longitudinal currents, and impedances allows one to obtain a complete equivalent circuit in terms of a (coupled) transmission line network.

References

[1] C. Wei, R. F. Harrington, J. R. Mautz, and T. K. Sarkar, "Multiconductor transmission lines in multilayered dielectric media," *IEEE Trans. Microwave Theory Tech.*, vol. MTT-32, pp. 439–450, Apr. 1984.

[2] Y. Fukuoka, Q. Zhang, D. Neikirk, and T. Itoh, "Analysis of multilayer interconnection lines for a high-speed digital integrated circuit," *IEEE Trans. Microwave Theory Tech.*, vol. MTT-33, pp. 527–532, June 1985.

[3] R. H. Jansen, "The spectral domain approach for microwave integrated circuits," *IEEE Trans. Microwave Theory Tech.*, vol. MTT-33, pp. 1043–1056, Oct. 1985.

[4] N. Faché and D. De Zutter, "Circuit parameters for single and coupled microstrip lines by a rigourous full wave space domain analysis," *IEEE Trans. Microwave Theory Tech.*, vol. 37, pp. 421–425, 1989.

[5] E. Sugita and O. Ibaragi, "Reliable multiwire circuits with small gauge wires," *IEEE Trans. Components, Hybrids, Manuf. Technol.*, vol. CHMT-2, pp. 532–536, Dec. 1979.

[6] G. Messner, "Cost-density analysis of interconnections," *IEEE Trans. Components, Hybrids, Manuf. Technol.*, vol. CHMT-10, pp. 143–151, June 1987.

[7] N. Faché and D. De Zutter, "Full-wave analysis of a perfectly conducting wire transmission line in a double layered conductor backed medium," *IEEE Trans. Microwave Theory Tech.*, vol. 37, pp. 512–518, Mar. 1989.

[8] H. Shibata and R. Terakado, "Characteristics of transmission lines with a single wire for a multiwire circuitboard," *IEEE Trans. Microwave Theory Tech.*, vol. MTT-32, pp. 360–364, Apr. 1984.

[9] H. Shibata and T. Koizumi, "Crosstalk of coupled transmission lines with round wires for a multiwire circuit board." *Trans. Inst. Electron. Commun. Eng. Japan*, vol. E69, pp. 1271–1274, Dec. 1986.

[10] A. J. Poggio and E. K. Miller, "Integral equation solutions of three-dimensional scattering problems," in *Computer Techniques for Electromagnetics*. New York: Pergamon Press, 1973, pp. 159–261.

[11] N. Faché, J. Van Hese, and D. De Zutter, "Generalised space domain Green's dyadic for multilayered media with special application to microwave interconnections," *J. Electromagn. Waves and Appl.*, vol. 3, no. 7, pp. 651–669, 1989.

[12] N. Faché, "High frequency analysis of two dimensional electrical interconnections," Ph.D. dissertation (in Dutch), University of Ghent, Belgium, Dec. 1989.

[13] N. Faché and D. De Zutter, "New high-frequency circuit model for coupled lossless and lossy waveguide structures," *IEEE Trans. Microwave Theory Tech.*, vol. 38, Mar. 1990.

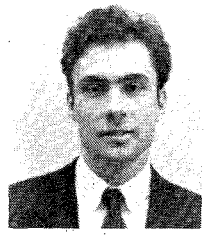

Niels Faché was born in Ghent, Belgium, on July 4, 1964. He received a degree in electrical engineering from the University of Ghent on July 1986. In December 1989 he obtained the Ph.D. degree from the Laboratory of Electromagnetism and Acoustics (LEA) at the University of Ghent. His research dealt with the full-wave analysis and circuit modeling of two-dimensional electrical interconnections embedded in multilayered media.

In 1990 he worked as a consultant from LEA to the Network Measurements Division (Santa Rosa, CA) of the Hewlett-Packard Company (HP). While at HP, he worked on the improvement of linear models in the Microwave Design System (MDS) and the implementation of new linear models. Currently, he is back at LEA, where his research now focuses on electromagnetic field solvers and their use in circuit simulators.

Frank Olyslager (S'90) was born in Wilrijk, Belgium, on November 24, 1966. He received a degree in electrical engineering from the University of Ghent in July 1989. At present he is work-

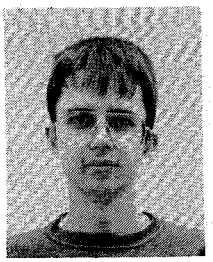

ing toward the Ph.D. degree in electrical engineering at the University of Ghent as a Research Assistant of the National Fund for Scientific Research of Belgium. His research concerns the electromagnetic modeling of high-frequency interconnections.

Daniël De Zutter was born in Eeklo, Belgium, on November 8, 1953. He received a degree in electrical engineering from the

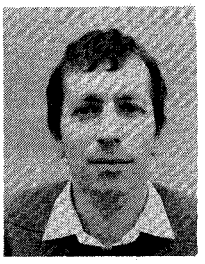

University of Ghent in July 1976. From September 1976 to September 1984 he was a research and teaching assistant in the Laboratory of Electromagnetism and Acoustics (LEA) at the same university. In October 1981 he obtained the Ph.D. degree there and in the spring of 1984 he completed a thesis leading to a degree equivalent to the French Aggrégation or the German Habilitation.

Most of his earlier scientific work dealt with the electrodynamics of moving media, with emphasis on the Doppler effect and the forces involved in the interaction of fields with moving media. At present he works a the LEA as a Research Associate of the National Fund for Scientific Research of Belgium. His research now focuses on all aspects of circuit and electromagnetic modeling of high-frequency and high-speed interconnections.